ACS Catalysis

Research Article

pubs.acs.org/acscatalysis

Kelvin Probe Force Microscopy in Surface Chemistry: Reactivity of Pd Nanoparticles on Highly Oriented Pirolytic Graphite

Elisa Palacios-Lidón,† Claude R. Henry, and Clemens Barth*

Aix-Marseille University, CNRS, CINaM UMR 7325, 13288 Marseille, France

Supporting Information

ABSTRACT: The reactivity of 10−50 nm large Pd nanoparticles (PdNPs) supported on the highly oriented pirolytic graphite (HOPG) surface has been studied under ultra-high-vacuum (UHV) conditions by monitoring the work function (WF) during Kelvin probe force microscopy. The WF of as-prepared PdNPs can vary by more than 600 meV under similar deposition conditions. Because of a chemical reaction between the PdNPs and the residual gas of the UHV at room temperature, the WF always continuously decreases until an equilibrium value is reached. We suspect carbon contamination resulting from the dissociation of CO and hydrocarbons for both phenomena. Smaller PdNPs exhibit a higher reactivity (contamination) than larger ones, and site effects can be observed. We show that annealing at high temperatures in an oxygen atmosphere is sufficient to obtain clean PdNPs, which exhibit the expected WF difference between HOPG and Pd.

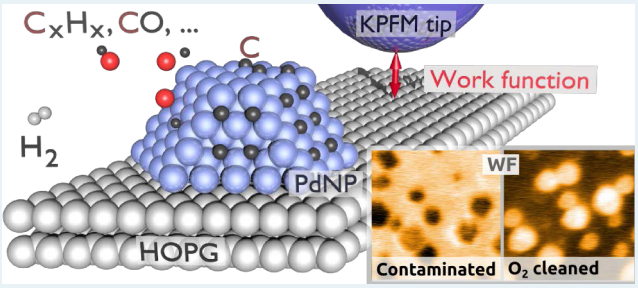

KEYWORDS: *Kelvin probe force microscopy, classical Kelvin probe, work function, heterogeneous catalysis, palladium nanoparticles, reactivity of nanoparticles, carbon contamination*

INTRODUCTION

Inspired by the classical Kelvin probe,[1,2] the Kelvin modulation technique was implemented as part of atomic force microscopy (AFM) in 1991 to measure the local work function (WF) of surfaces.[3,4] Since then, Kelvin probe force microscopy (KPFM) has been used for many applications in surface science and nanosciences because of its high resolution at the nanometer and atomic scale[5] and in the Kelvin voltage.[6,7] KPFM is mostly applied during noncontact AFM (nc-AFM) imaging,[7−9] in the frequency[10] or amplitude mode,[11] which permits quantifying WF differences of different conductors on surfaces,[4,12,13] and of thin insulating films[14−17] and supported molecules on conducting surfaces.[18−20]

KPFM measurements that permit extraction of quantitative values of either the absolute surface WF or WF differences of different materials on one and the same surface have created a strong demand for KPFM. To determine the absolute surface WF, the tip first needs to be calibrated by a measurement on a reference surface [e.g., on the highly oriented pirolytic graphite (HOPG) surface[21−23]], which has a well-known WF. However, the WF of the tip is not needed if WF differences of different materials on a surface are measured, as long as the WF of one material is known.

In any quantitative KPFM measurement, the WF of the reference needs to be well-defined. However, this is sometimes quite challenging because surfaces are subject to chemical reactions, which may change the surface WF even under UHV conditions.[24] This has been previously stated in the first KPFM work, which found that the WF difference between adjacent thick gold and palladium films varies over time due to adsorbates,[4] a contamination phenomenon recently observed also on the HOPG surface in air under ambient conditions.[25] The sensitivity of KPFM to the surface chemistry becomes clear when considering its older sister technique, classical Kelvin probe,[1,2] which has been used to explicitly analyze catalytic reactions.[24] A great success was realized in surface chemistry as exemplified by Gerhard Ertl's key work on the famous CO/CO_2 oscillations on crystalline platinum or palladium surfaces.[26,27]

In this work, we focus on two important aspects in KPFM and surface chemistry. On one hand, we show that utmost care needs to be taken when preparing supported metal nanoparticles (NPs) with well-defined WFs, in particular palladium NPs (PdNPs). On the other hand, we discuss the important role of KPFM in surface chemistry, with its potentially strong capacity to visualize the reactivity of metal NPs. We discuss both aspects by presenting results for high-temperature PdNPs grown on the HOPG surface, which were prepared and imaged by nc-AFM and KPFM in UHV. PdNPs are relevant in heterogeneous model catalysis[28,29] even on carbon substrates,[30,31] and metal NPs on HOPG in general are suitable samples for studying the growth of the NPs[32−34] and for testing the imaging in nc-AFM[35] and KPFM.[13]

Received: February 10, 2014
Revised: April 18, 2014
Published: April 25, 2014

 © 2014 American Chemical Society

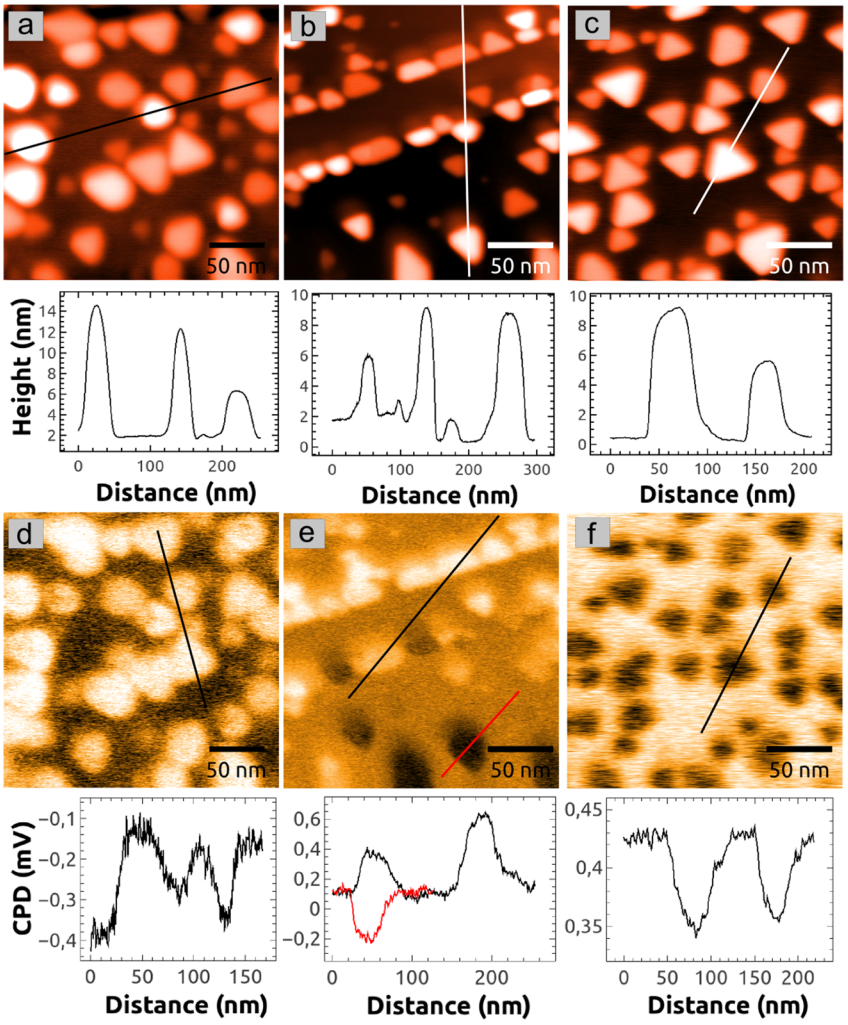

Figure 1. PdNPs typically a few hours after their growth at high temperatures on three separate HOPG sample surfaces [PD quantities of 3 ML (a), 3 ML (b), and 4 ML (c) (ML denotes monolayers) and T_{growth} values of 413 °C (a), 380 °C (b), and 447 °C (c)]. The topography images are shown in the top row (a–c) and the Kelvin images in the bottom row (d–f). A profile was obtained at the position of the line from the respective image above. Image sizes of 250 nm × 250 nm (a) and 300 nm × 300 nm (b and c).

RESULTS

The three topography images in panels a–c of Figure 1 show three-dimensional (3D) PdNPs, which were grown on three separate HOPG surfaces at high temperatures. Because of their 3D shape of a top-truncated tetrahedron and their $(111)_{Pd}\|(00.1)_{HOPG}$ and $[11\bar{2}]_{Pd}\|[1\bar{1}.0]_{HOPG}$ epitaxial orientation, the PdNPs exhibit well-known shapes from triangles to regular hexagons via various truncated shapes, with the PdNPs' edges always forming angles of 60° and 120°.[33] The top facets are atomically flat and are in their (111) surface orientation, with the side facets in (111) and (001) orientations.[33] The side lengths of the PdNPs can vary between 10 and 50 nm, whereas their height can reach values of up to 10 nm and occasionally higher.

Very interesting contrast features can be seen when analyzing the corresponding Kelvin images d–f in Figure 1, which were acquired simultaneously with topography images a–c, respectively: the PdNPs can exhibit either a bright or dark contrast with respect to the HOPG surface. In image d, the difference in the CPD [contact potential difference (see the Experimental Section)] between the PdNPs and HOPG is positive ($\Delta CPD_{Pd\text{-}HOPG} \approx 250$ mV), and a positive ΔCPD value of almost all PdNPs could also be found on the second surface shown in Figure 1e (top NP row, $\Delta CPD_{Pd\text{-}HOPG} \approx 500$ mV; NPs in the middle, $\Delta CPD_{Pd\text{-}HOPG} \approx 250$ mV). Interestingly, a few NPs exhibit a strong dark Kelvin contrast ($\Delta CPD_{Pd\text{-}HOPG} \approx -300$ mV), whereas no particular contrast features at the same NPs are visible in the corresponding topography image (image b). We assign this dark contrast at single PdNPs to a lower WF, which was probably influenced by surface defects underneath the NPs.[36]

In contrast to the previous two surfaces, we observed on the third for all NPs an exclusively dark Kelvin contrast (Figure 1f), which corresponds in mean to $\Delta CPD_{Pd\text{-}HOPG} \approx -80$ mV. In general, we never observed $\Delta\phi_{Pd\text{-}HOPG,min}$ values less than approximately −150 meV for such dark PdNPs.

Because the CPD difference is directly related to the WF difference ($\Delta CPD_{Pd\text{-}HOPG} = \Delta\phi_{Pd\text{-}HOPG}/e$), bright PdNPs obviously have a higher WF than HOPG and vice versa (see also below). The WF difference $\Delta\phi_{Pd\text{-}HOPG}$ can vary from growth to growth, in a manner independent of the preparation parameters like the partial pressure of the UHV during the growth of the PdNPs ($p_{tot} = 1-3 \times 10^{-9}$ mbar). An analysis of results obtained for all our samples shows that we rarely obtain values around $\Delta\phi_{Pd\text{-}HOPG} = 500$ meV or values that are negative

dx.doi.org/10.1021/cs500177h | ACS Catal. 2014, 4, 1838–1844

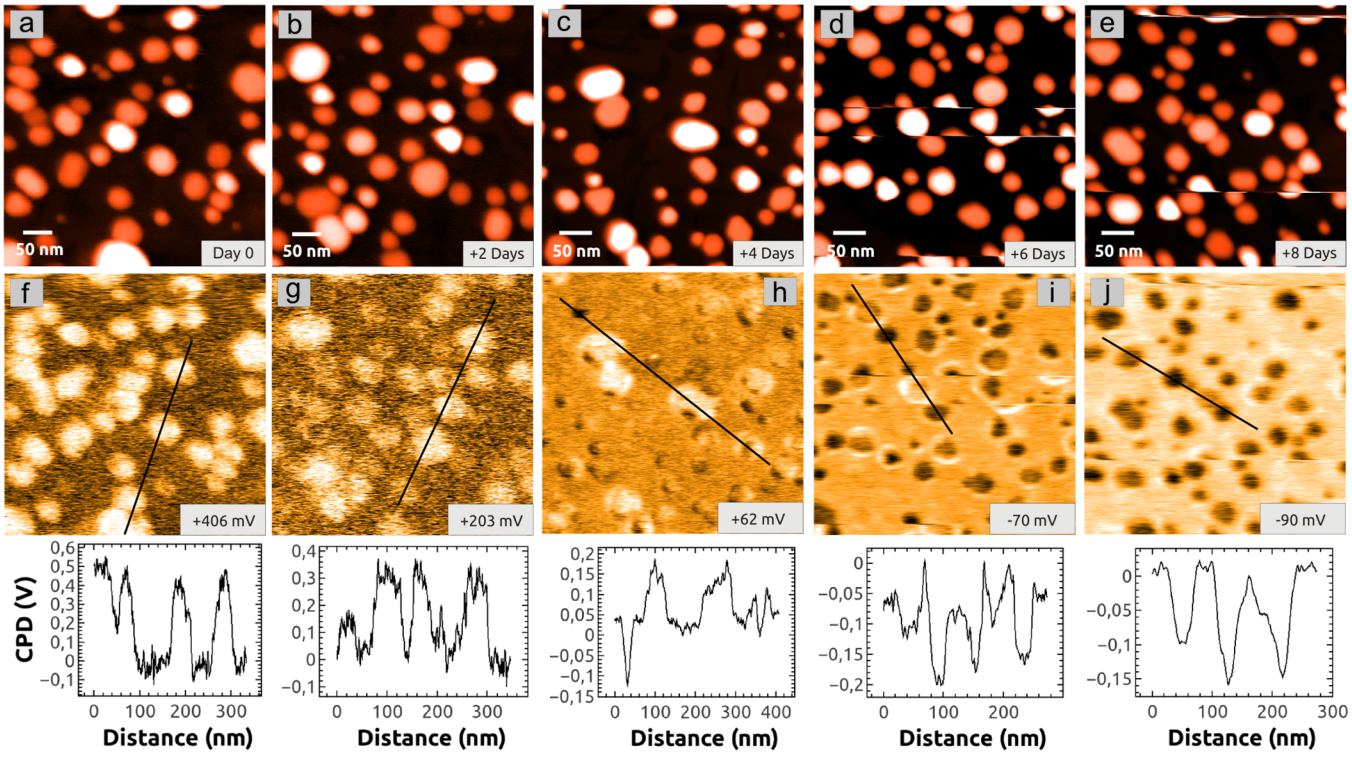

Figure 2. Temporal evolution of PdNPs on a HOPG surface during observation over 8 days (quantity of 3 ML, T_{growth} value of 413 °C). The topography images are shown in the top row (a–e) and the Kelvin images in the bottom row (f–j). A Kelvin profile was obtained at the position of the line in the respective Kelvin image above. Image sizes of 400 nm × 400 nm.

($\Delta\phi_{Pd\text{-}HOPG} < 0$ V). In most cases, we observe a higher WF for the PdNPs than for the HOPG surface, however, with values of $\Delta\phi_{Pd\text{-}HOPG}$, which are lower than the expected value for the WF difference between Pd(111) and HOPG [$\Delta\phi_{Pd(111)\text{-}HOPG} = \phi_{Pd(111),lit} - \phi_{HOPG,lit}$ = 5.5–5.0 eV = 500 meV (see the Experimental section for the choice of WF values for HOPG and the PdNPs)]. Note that we use the absolute WF of Pd(111) single-crystal surfaces because the PdNPs are large enough to assume bulk electronic properties.

From our results, one can conclude that as-grown PdNPs cannot be used as a good WF reference in KPFM. Note that annealing experiments at high temperatures in UHV ($p_{tot} < 3 \times 10^{-10}$ mbar) failed to produce the expected WF difference $\Delta\phi_{Pd(111)\text{-}HOPG}$ for PdNPs with an initial low WF. The expected WF difference could also not be obtained when dosing with oxygen, hydrogen, and CO during the scanning at room temperature (typical partial pressure of 10^{-7} mbar, several tens of Langmuir). As discussed below, the small WF differences observed in Figure 1 are due to a contamination of the PdNPs with carbon via the dissociation of a carbon-containing gas like carbon monoxide. Although the base pressure p_{tot} is almost the same for each deposition experiment, the partial pressure of, e.g., carbon monoxide can vary from deposition to deposition, in particular above the sample surface, which explains the observations in Figure 1.[37]

A second important key observation of our KPFM work concerns the temporal development of the NP work function, which we found to be independent of the initial WF value of the NPs after their growth. Figure 2 shows an image series of PdNPs, which were annealed in oxygen (see below) before the series started. The images were obtained on one and the same sample surface within a period of 8 days, imaged under the same imaging conditions. The NPs were not treated by additional annealing or gas dosage experiments during the 8 days; they were merely exposed to the residual gas of the UHV ($p_{tot} = 4 \times 10^{-10}$ mbar), which contained hydrogen, water, CO, and CO_2 as the main constituents (see the Supporting Information). Because of the drift of the AFM scanner, it was not possible to keep the tip in the same region of the sample. However, the images in Figure 2 always show typical features of the PdNPs.

During the observation period of 8 days, we could not detect any changes in the shape of the particles (see topography images). The Kelvin images, however, show large changes in the relative contrast: on the first day (image f), the PdNPs exhibit a bright Kelvin contrast with respect to the HOPG surface, which corresponds to a mean CPD difference of $\Delta CPD_{Pd\text{-}HOPG}$ = 406 mV. After ∼2 days (image g), the NPs become less bright ($\Delta CPD_{Pd\text{-}HOPG}$ = 203 mV) and have, after 4 days (image h), a contrast similar to that of HOPG ($\Delta CPD_{Pd\text{-}HOPG}$ = 62 mV). In the latter two images, it can be clearly seen that smaller PdNPs exhibit a contrast that is less bright than that of larger NPs. In particular, the large NPs in image h have a bright contrast and the small NPs a dark one. After ∼6 and ∼8 days (images i and j, respectively), all PdNPs are dark with corresponding $\Delta CPD_{Pd\text{-}HOPG}$ values of −70 and −90 mV, respectively. Note that although the WF is uniformly distributed over the PdNPs, in particular on the top facets (see the Supporting Information), we occasionally observe also site effects, which can be clearly seen in images h and i: a dark contrast (lower WF) can be found at the edges of the largest NPs in image h, whereas a bright fringe (higher WF) can be found at a few NPs in image i.

Figure 3 shows the temporal decrease in the mean $\Delta CPD_{Pd\text{-}HOPG}$ of the measurements shown in Figure 2 (dark circles). The maximal and minimal values (error bars) are

dx.doi.org/10.1021/cs500177h | ACS Catal. 2014, 4, 1838–1844

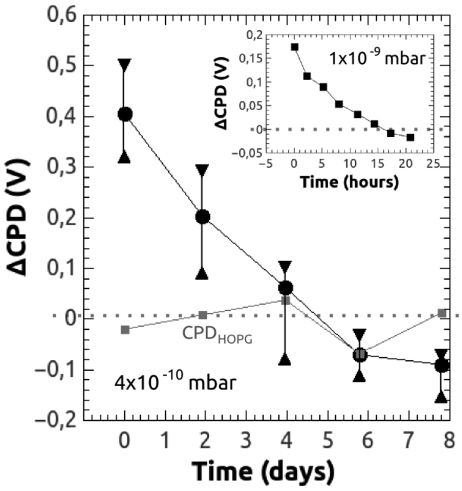

Figure 3. Temporal evolution of the CPD difference, $\Delta CPD_{Pd-HOPG}$, of the PdNPs in Figure 2. The mean (●), minimal (▲), and maximal (▼) values are shown. The mean CPD between the tip and HOPG surface is represented by the gray squares. The inset shows the temporal evolution of the CPD difference for other PdNPs, which were exposed to a residual gas at a higher pressure.

shown at the same time and correspond basically to the $\Delta CPD_{Pd-HOPG}$ values of large and small PdNPs, respectively. We also show the mean values of the CPD between the AFM tip and HOPG surface (gray squares), which are all close to zero CPD (CPD ≈ 6 mV). This is important information because it shows that the WF of the tip did not change much during the acquisition of the images in Figure 2. In other words, the contrast changes in the Kelvin images of Figure 2 are due to changes in the work function of the PdNPs. Because we cannot directly verify this for the small WF differences observed at the PdNPs directly after their preparation (Figure 1), we assume that it is the PdNPs, which have a small WF already from the beginning of the growth, whereas the HOPG surface is always at its expected $\phi_{HOPG,lit}$ value of ∼5.0 eV.

In Figure 3, a second curve (inset) shows the temporal WF evolution of other PdNPs, which were exposed to an ∼2-fold higher base pressure of the UHV ($p_{tot} = 1 \times 10^{-9}$ mbar). After only 1 day, the PdNPs are dark in comparison to HOPG; the decrease in the work function of the NPs obviously scales with the base pressure of the UHV. Once the PdNPs have decreased their WF to a mean saturation $\Delta\phi_{Pd-HOPG,min}$ value of −150 meV, no further changes in the WF can be observed; the PdNPs have reached a stable electronic configuration in UHV.

To obtain the expected WF difference between the HOPG surface and the PdNPs, we have annealed the NPs in an oxygen (O_2) environment. For many oxygen annealing treatments, we have chosen typical values of 500 °C, 30 min, and 5×10^{-6} mbar for the temperature, time, and oxygen partial pressure, respectively. In all cases, we could considerably increase the work function of the PdNPs; one example is shown in Figure 4. The PdNPs, which can be seen in topography image a and Kelvin image b, were left for almost 5 days after their preparation in the UHV chamber and have a CPD difference of $\Delta CPD_{Pd-HOPG}$ = −150 mV with respect to HOPG. After the sample had been annealed in oxygen, the CPD of the PdNPs drastically increased such that a CPD difference of $\Delta CPD_{Pd-HOPG}$ ≈ 600 mV could be measured, a typical value we also found for other oxygen-annealed samples. This value is much closer to the expected value between Pd(111) and

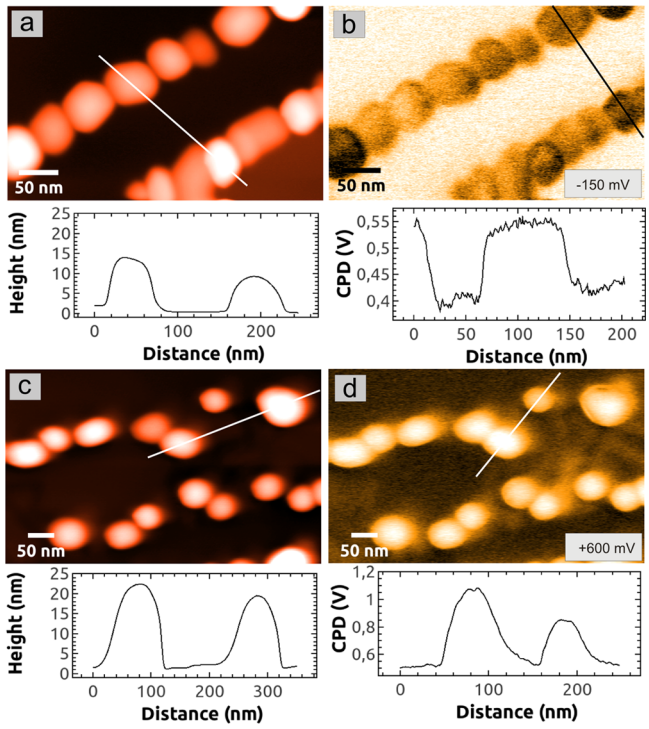

Figure 4. PdNPs on HOPG before (a and b) and after (c and d) being annealed in 6×10^{-6} mbar oxygen at 517 °C for 30 min. Images a and c and images b and d represent the topography and Kelvin voltage, respectively. The measurement (a and b) was obtained 4.87 days after the preparation of the NPs (quantity of 3 ML, T_{growth} value of 425 °C). Image sizes of 400 nm × 245 nm (a and b) and 600 nm × 368 nm (c and d).

HOPG [$\Delta\phi_{Pd(111)-HOPG}$ = 500 meV]. As discussed in the next section, the PdNPs are "cleaned" by oxygen at high temperatures and are composed of clean palladium, which can then be used as a WF reference.

Note that the difference of 100 mV with respect to the expected literature value of $\Delta\phi_{Pd(111)-HOPG}$ might be due to our HOPG samples having a slightly lower WF of ϕ_{HOPG} = 4.9 eV in comparison to the value of 5.0 eV obtained previously by KPFM.[21,22] In the previous KPFM studies, the HOPG surface was cleaved in UHV; here the samples were cleaved in air, immediately transferred into the UHV chamber, and annealed at high temperatures in UHV afterward.

Two accompanying effects of an oxygen annealing can be observed: the morphology of the PdNPs changes such that their shape is no longer triangular but round. Furthermore, the height of the PdNPs is increased as it can be seen in the topography profiles of both experiments in Figure 4. We exclude the possibility that the PdNPs become oxidized during the oxygen annealing because the partial oxygen pressure is still too low at the temperatures we used.[38,39] The change in the equilibrium shape of the PdNPs is rather a known process of the oxygen chemisorption energy, which is stronger on the (001) facets than on the (111) facets: the (001) facets extend and the (111) facets shrink because of a stronger adsorption of oxygen on the more open (100) facets, which leads to the rounding of the NPs as previously observed with gold,[40,41] platinum,[42] and palladium NPs.[43] The second accompanying effect concerns the oxidation of the HOPG at the periphery with the PdNPs, which function as a catalyst.[44] We observed pits and long channels in the surface, which is, however, not

dx.doi.org/10.1021/cs500177h | ACS Catal. 2014, 4, 1838−1844

relevant in the context of the WF of the systems. More details can be found in the Supporting Information.

DISCUSSION

Because the decrease in the WF difference at room temperature (RT) scales with the partial pressure of the UHV, obvious sources at first glance are the constituents of the residual gas of the UHV. Candidates are hydrogen, carbon monoxide, carbon dioxide, and water, which could change in principle the WF by adsorbing on the facets of the PdNPs. Apart from carbon dioxide, which does not adsorb at all on palladium at RT, the WF change induced by almost any relevant gas has been extensively studied in the past by the classical Kelvin probe technique, in particular on palladium single-crystal surfaces. At RT, dosed oxygen (O_2), hydrogen (H_2), and carbon monoxide all increase the WF of the Pd(111) surface at low pressures by $\Delta\phi \approx 800$ meV,[45] $\Delta\phi \approx 110$ meV,[46] and $\Delta\phi \approx 850$ meV,[47] respectively (note that oxygen and hydrogen dissociatively adsorb on the surface[38,39,46]). The WF change is "quickly" reached after a dosage between some and few tens of Langmuir only, and a WF increase is also always observed at much higher temperatures. The only candidate so far, which can be found in any residual gas of the UHV and which decreases the WF of metals in general, is water.[48] For instance, water on 8−100 nm thick palladium films can decrease the surface WF by up to $\Delta\phi \approx -800$ meV,[49] which is also supported by theory considering water on the perfect Pd(111) surface ($\Delta\phi \approx -1.22$ eV[50]). However, it is also known that water adsorbs only at relatively low temperatures:[49] for instance, a recent X-ray photoelectron spectroscopy work shows that water is stable only until a temperature of 180 K.[51] This is due to the fact that, in general, the adsorption energy of water on metal surfaces is relatively low:[52] E_a values from ≈0.2 eV[50] to 0.3 eV (monomer) and an E_a of ≈0.5 eV/molecule (half-dissociated water bilayer) were calculated on the perfect Pd(111) surface.[53] A rough estimation of the adsorption time (1 Langmuir of H_2O is adsorbed within 24 h at $p_{H_2O} = 1 \times 10^{-11}$ mbar; sticking coefficient = 1) clearly indicates that it also seems unreasonable to assume that water explains the extremely slow WF reduction of the PdNPs over several days. Even if water dissociates leaving behind hydroxyls on the facets, the WF should increase.[48] The most important argument against water is that annealing at elevated temperatures should desorb a possible water layer on the facets such that the work function of the PdNPs increases, which is, however, not supported by our annealing experiments.

Because no potential candidate of the residual gas can be found, it can be assumed that "impurity species" are probably adsorbed on or built into the PdNPs over time via the decomposition of adsorbed gases from the UHV, modifying the work function of the NPs. Without any direct evidence, we suspect hydrogen and, in particular, carbon, which are adsorbed on or dissolved inside the PdNPs. Both atomic components can be principally obtained by dissociation of molecular hydrogen, carbon monoxide, or hydrocarbon gas, in particular, at low-coordinated sites (e.g., kinks and steps of facets) as discussed for carbon monoxide.[54−56] Because this is a quite rate limiting process, it would explain the extremely long decrease in the WF over many hours and even days. Furthermore, it could explain also the enhanced contrast at the NPs edges we rarely observed in the few Kelvin images (Figure 2h,i). More importantly, a preferred reaction at weakly coordinated sites also means that small NPs are more reactive because they have a larger number of low-coordinated sites per surface area than larger NPs, as experimentally evidenced previously.[54,55] In other words, we could directly observe a higher reactivity of small PdNPs in our Kelvin images (Figure 2) via imaging stronger WF changes by KPFM.

An adsorption of both impurities can be assumed to take place on the facets of the NPs, which follows for carbon from Auger electron spectroscopy, core electron energy loss spectroscopy, and static secondary ion mass spectroscopy.[54,57] However, as recently shown, both can also be located inside the NPs in a subsurface region.[58,59] Note that in general, carbon prefers to migrate from the surface to a subsurface region of a Pd(111) surface[60] or even a PdNP facet.[61]

The most important question is whether hydrogen or carbon is indeed responsible for the decrease in the WF of the NPs. It is widely accepted in surface science that palladium single-crystal surfaces have to be cleaned prior to adsorption experiments by being annealed in oxygen (see, e.g., refs 45−47 and 49). In some classical Kelvin probe work, it is stated that carbon is the main impurity and that the cleanness of the palladium surface is mostly reached when the WF is maximal,[46,62] a signature that carbon reduces the WF of palladium. A recent work about PdNP catalysts even states that dissolved carbon decreases the work function of the NPs and that oxygen annealing cleans the NPs.[63]

Without excluding the role of atomic hydrogen inside the NPs,[58,59] we suspect in particular carbon either adsorbed on or dissolved in our PdNPs, reducing the WF of the NPs. The long time needed to dissociate carbon-containing gas explains qualitatively the very slow reduction of the work function of the PdNPs. Our observation that an oxygen annealing is needed to obtain the expected WF of palladium further supports the picture of the removal of carbon from the PdNPs.

CONCLUSION

Up to 50 nm large palladium nanoparticles (PdNPs) in their (111) geometry have been grown in UHV on the HOPG surface at high temperatures (370−470 °C) and have been studied by *in situ* nc-AFM and frequency-modulated KPFM. In a manner that independent of the partial pressure (~5×10^{-10} mbar) during the growth of the NPs, the WF of the PdNPs may exhibit variations of up to 600 mV from preparation to preparation. Irrespective of the initial WF value of the PdNPs, the WF decreases on a time scale of days below the WF of the HOPG surface, which remains constant over the period. The WF decreases until a saturation value at $\Delta\phi_{\text{Pd-HOPG,min}} = -150$ meV ($\phi_{\text{Pd,min}} \approx 4.75$ eV) is reached. KPFM exhibits a higher reactivity of small NPs in comparison to larger ones and also reveals site effects at single NPs. When the PdNPs are annealed in an oxygen environment (10^{-6} mbar) at a high temperature (500 °C), the expected WF change of $\Delta\phi_{\text{Pd-HOPG}} \approx 600$ meV between the PdNPs and HOPG is obtained. We anticipate that impurities like carbon from the residual gas of the UHV (via dissociation of CO and hydrocarbons) are adsorbed on or dissolved in the NPs such that the WF of palladium is decreased. Annealing in oxygen cleans the PdNPs by removing the contamination species.

Our work comprises the important finding that PdNPs, and probably similar metal NPs like platinum group NPs, have to be cleaned in the standard fashion by being annealed in oxygen prior to quantitative WF measurements, in particular when such NPs are used as a reference in KPFM. It further demonstrates that KPFM can be used to visualize and quantify phenomena

dx.doi.org/10.1021/cs500177h | ACS Catal. 2014, 4, 1838−1844

related to surface chemistry at the nanometer scale, by measuring WF changes with millivolt resolution, which was done by its older sister technique, classical Kelvin probe. Our work creates a new general perspective in heterogeneous model catalysis to use KPFM as a standard surface science tool for reactivity studies at single NPs. In the future, we will focus on important reactivity experiments in model catalysis like the hydrogenation of hydrocarbons at PdNPs.

EXPERIMENTAL SECTION

Noncontact AFM and KPFM experiments were performed in an ultrahigh vacuum (UHV) chamber (10^{-10} mbar base pressure)[64] with an Omicron RT-AFM/STM instrument (digital demodulator, NanoSurf) at RT. Conducting silicon cantilevers with resonance frequencies of 70 kHz (Nanosensors PPP-QFMR, p-Si, 0.015 Ω cm) were used, with the oscillation amplitude kept constant at a few nanometers. In frequency-modulated KPFM,[10,65] a dc voltage (U_{dc}) and ac voltage (U_{ac}) with frequency f_{ac} are applied between the sample and tip. In our experiments, the voltages are applied at the sample and the tip is grounded. The electrostatic tip−surface interaction is minimized at each point on the surface by the dc voltage, which yields the contact potential difference (CPD) between the tip and surface: CPD = $U_{dc,0} = (\phi_{sample} - \phi_{tip})/e$. If at two different locations on the surface (positions 1 and 2) the CPD is measured, the CPD difference $\Delta CPD = CPD_1 - CPD_2 = [(\phi_1 - \phi_{tip}) - (\phi_2 - \phi_{tip})]/e = (\phi_1 - \phi_2)/e = \Delta\phi/e$ yields the work function difference $\Delta\phi_{1-2} = \phi_1 - \phi_2$ between the two surface locations[10] (Kelvin contrast). KPFM is applied during the normal topography imaging so that a topography and Kelvin image of $U_{dc,0}$ are simultaneously obtained. In our setup, a bright contrast in a Kelvin image corresponds to a high WF and vice versa. Typical values for the ac voltage (U_{ac}) and frequency f_{ac} are 150−300 mV and 450 Hz, respectively. Images were acquired with the Omicron SCALA system and analyzed with Gwyddion.[66]

Fresh surfaces were prepared by cleaving HOPG samples in air and quickly transferred afterward into the UHV chamber within a few minutes. Inside the UHV chamber, the graphite samples were cleaned by being annealed for several hours in an UHV oven[64] kept at 550 °C. The PdNPs were grown by evaporating neutral palladium atoms from a Knudsen cell with a calibrated deposition rate of 0.45 ML/min onto the HOPG sample, which was located in the UHV oven. With the variation of the deposition time, coverages with a nominal thickness between 2 and 5 ML were obtained, which resulted in 10−50 nm NPs. During the growth, the HOPG substrate was held at a constant temperature in the T_{growth} range of 350−450 °C to guarantee well-faceted PdNPs. Caution was taken such that the pressure never exceeded 10^{-9} mbar. After the preparation of the NPs, the samples were cooled and imaged afterward by AFM at RT.

For the absolute WF of HOPG and the PdNPs in their (111) epitaxy (see below), we use $\phi_{HOPG,lit}$ = 5.0 eV and $\phi_{Pd(111),lit}$ = 5.50 eV, respectively, which yields the WF difference of $\phi_{Pd(111)\text{-}HOPG}$ = 500 meV. The value for HOPG is a mean value from values previously obtained by UHV experiments and theory (experimental values of 5.0 eV[22] and 5.0 eV;[21] calculated values of 4.4−5.2 eV[67]). In the case of the PdNPs, we use the absolute WF of the Pd(111) single-crystal surface because the PdNPs are still large enough to assume bulk electronic properties. The absolute WF value for Pd(111) is also a mean value of literature values (experimental values of 5.6 eV,[68] 5.50 eV,[69] 5.46 eV,[70] and 5.55 eV;[71] calculated values of 5.53 eV[72] and 5.42 eV[73]).

ASSOCIATED CONTENT

Supporting Information

Details about the preparation of samples and supporting experiments. This material is available free of charge via the Internet at http://pubs.acs.org.

AUTHOR INFORMATION

Corresponding Author

*E-mail: barth@cinam.univ-mrs.fr.

Present Address

†E.P.-L.: Departamento de Física, Edificio CIOyN, Campus Espinardo, Universidad de Murcia, E-30100 Murcia, Spain.

Notes

The authors declare no competing financial interest.

ACKNOWLEDGMENTS

Stimulating discussions with J. Niebauer and Ch. Bichara are gratefully acknowledged. We also acknowledge the French agency for Research (Agence Nationale pour la Recherche, ANR) for financial support through programs CANA and MISS and the European COST for financial support through action D41.

REFERENCES

(1) Kelvin, L.; Fitzgerald, G.; Francis, W. *Philos. Mag. (1798−1977)* **1898**, *46*, 82−120.
(2) Zisman, W. A. *Rev. Sci. Instrum.* **1932**, *3*, 367−370.
(3) Weaver, J. M. R.; Abraham, D. W. *J. Vac. Sci. Technol., B: Nanotechnol. Microelectron.: Mater., Process., Meas., Phenom.* **1991**, *9*, 1559−1561.
(4) Nonnenmacher, M.; O'Boyle, M. P.; Wickramasinghe, H. K. *Appl. Phys. Lett.* **1991**, *58*, 2921−2923.
(5) Sadewasser, S.; Jelinek, P.; Fang, C. K.; Custance, O.; Yamada, Y.; Sugimoto, Y.; Abe, M.; Morita, S. *Phys. Rev. Lett.* **2009**, *103*, 266103.
(6) Melitz, W.; Shen, J.; Kummel, A. C.; Lee, S. *Surf. Sci. Rep.* **2011**, *66*, 1−27.
(7) Barth, C.; Foster, A. S.; Henry, C. R.; Shluger, A. L. *Adv. Mater.* **2011**, *23*, 477−501.
(8) Morita, S.; Wiesendanger, R.; Meyer, E. *Noncontact Atomic Force Microscopy*; Springer-Verlag: Berlin, 2002.
(9) Morita, S.; Giessibl, F.; Wiesendanger, R. *Noncontact Atomic Force Microscopy*; Springer-Verlag: Berlin, 2009.
(10) Kitamura, S.; Iwatsuki, M. *Appl. Phys. Lett.* **1998**, *72*, 3154−3156.
(11) Kikukawa, A.; Hosaka, S.; Imura, R. *Rev. Sci. Instrum.* **1996**, *67*, 1463−1467.
(12) Goryl, M.; Krok, F.; Kolodziej, J. J.; Piatkowski, P.; Such, B.; Szymonski, M. *Vacuum* **2004**, *74*, 223−227.
(13) Glatzel, T.; Sadewasser, S.; Lux-Steiner, M. C. *Appl. Surf. Sci.* **2003**, *210*, 84−89.
(14) Loppacher, C.; Zerweck, U.; Eng, L. M. *Nanotechnology* **2004**, *15*, S9−S13.
(15) Zerweck, U.; Loppacher, C.; Otto, T.; Grafström, S.; Eng, L. M. *Phys. Rev. B* **2005**, *71*, 125424.
(16) Bieletzki, M.; Hynninen, T.; Soini, T. M.; Pivetta, M.; Henry, C. R.; Foster, A. S.; Esch, F.; Barth, C.; Heiz, U. *Phys. Chem. Chem. Phys.* **2010**, *12*, 3203−3209.
(17) Cabailh, G.; Henry, C. R.; Barth, C. *New J. Phys.* **2012**, *14*, 103037.
(18) Palacios-Lidón, E.; Abellán, J.; Colchero, J.; Munuera, C.; Ocal, C. *Appl. Phys. Lett.* **2005**, *87*, 154106.
(19) Perez-Garcia, B.; Abad, J.; Urbina, A.; Colchero, J.; Palacios-Lidon, E. *Nanotechnology* **2008**, *19*, 065709.

(20) Palacios-Lidón, E.; Pérez-Garca, B.; Colchero, J. *Nanotechnology* **2009**, *20*, 085707.
(21) Bohmisch, M.; Burmeister, F.; Rettenberger, A.; Zimmermann, J.; Boneberg, J.; Leiderer, P. *J. Phys. Chem. B* **1997**, *101*, 10162−10165.
(22) Sommerhalter, C.; Matthes, T. W.; Glatzel, T.; Jäger-Waldau, A.; Lux-Steiner, M. C. *Appl. Phys. Lett.* **1999**, *75*, 286−288.
(23) Kim, C. H.; Bae, C. D.; Ryu, K. H.; Lee, B. K.; Shin, H. J. *Solid State Phenom.* **2007**, *124*, 607−610.
(24) Kim, C. H.; Bae, C. D.; Ryu, K. H.; Lee, B. K.; Shin, H. J. *Introduction to Surface Chemistry and Catalysis*; John Wiley & Sons, Inc.: New York, 1994.
(25) Martinez-Martin, D.; Longuinhos, R.; Izquierdo, J. G.; Marele, A.; Alexandre, S. S.; Jaafar, M.; Gómez-Rodríguez, J. M.; Bañares, L.; Soler, J. M.; Gomez-Herrero, J. *Carbon* **2013**, *61*, 33−39.
(26) Ertl, G.; Norton, P. R.; Rüstig, J. *Phys. Rev. Lett.* **1982**, *49*, 177−180.
(27) Ladas, S.; Imbihl, R.; Ertl, G. *Surf. Sci.* **1989**, *219*, 88−106.
(28) Libuda, J.; Freund, H.-J. *Surf. Sci. Rep.* **2005**, *57*, 157−298.
(29) Henry, C. R. *Surf. Sci. Rep.* **1998**, *31*, 231−325.
(30) Tardy, B.; Noupa, C.; Leclercq, C.; Bertolini, J. C.; Hoareau, A.; Treilleux, M.; Faure, J. P.; Nihoul, G. *J. Catal.* **1991**, *129*, 1−11.
(31) Rousset, J. L.; Cadrot, A. M.; Cadete Santos Aires, F. J.; Renouprez, A.; Mélinon, P.; Perez, A.; Pellarin, M.; Vialle, J. L.; Broyer, M. *J. Chem. Phys.* **1995**, *102*, 8574−8585.
(32) Piednoir, A.; Perrot, E.; Granjeaud, S.; Humbert, A.; Chapon, C.; Henry, C. R. *Surf. Sci.* **1997**, *391*, 19−26.
(33) Chapon, C.; Granjeaud, S.; Humbert, A.; Henry, C. R. *Eur. Phys. J.: Appl. Phys.* **2001**, *13*, 23−30.
(34) Hövel, H.; Barke, I. *Prog. Surf. Sci.* **2006**, *81*, 53−111.
(35) Barth, C.; Pakarinen, O. H.; Foster, A. S.; Henry, C. R. *Nanotechnology* **2006**, *17*, S128−S136.
(36) Pong, W.-T.; Durkan, C. *J. Phys. D: Appl. Phys.* **2005**, *38*, R329.
(37) The partial pressure of CO and other relevant gases was measured by a QMS, which is located above the housing of the oven (see the Experimental Section), without direct access to the sample inside the oven. The partial pressure of a specific gas does therefore not represent the corresponding local partial pressure on the sample surface during the preparation. The latter can be quite different because the Knudsen cell and the UHV oven are out-gazing during a preparation, and the partial pressure of a specific gas on the sample surface can vary from preparation to preparation.
(38) Banse, B. A.; Koel, B. E. *Surf. Sci.* **1990**, *232*, 275−285.
(39) Penner, S.; Bera, P.; Pedersen, S.; Ngo, L. T.; Harris, J. J. W.; Campbell, Ch. T. *J. Phys. Chem. B* **2006**, *110*, 24577−24584.
(40) Gai, P. L.; Boyes, E. D.; Helveg, S.; Hansen, P. L.; Giorgio, S.; Henry, C. R. *MRS Bull.* **2007**, *32*, 1044−1050.
(41) Giorgio, S.; Cabie, M.; Henry, C. R. *Gold Bull. (Berlin, Ger.)* **2008**, *41*, 167−173.
(42) Cabié, M.; Giorgio, S.; Henry, C. R.; Axet, M. R.; Philippot, K.; Chaudret, B. *J. Phys. Chem. C* **2010**, *114*, 2160−2163.
(43) Giorgio, S.; Sao Joao, S.; Nitsche, S.; Chaudanson, D.; Sitja, G.; Henry, C. R. *Ultramicroscopy* **2006**, *106*, 503−507.
(44) Baker, R. T. K.; France, J. A.; Rouse, L.; Waite, R. J. *J. Catal.* **1976**, *41*, 22−29.
(45) Surnev, L.; Bliznakov, G.; Kiskinova, M. *Surf. Sci.* **1984**, *140*, 249−260.
(46) Conrad, H.; Ertl, G.; Latta, E. E. *Surf. Sci.* **1974**, *41*, 435−446.
(47) Conrad, H.; Ertl, G.; Koch, J.; Latta, E. E. *Surf. Sci.* **1974**, *43*, 462−480.
(48) Thiel, P. A.; Madey, T. E. *Surf. Sci. Rep.* **1987**, *7*, 211−385.
(49) Heras, J. M.; Estiu, G.; Viscido, L. *Appl. Surf. Sci.* **1997**, *108*, 455−464.
(50) Cao, Y.; Chen, Z.-X. *Phys. Chem. Chem. Phys.* **2007**, *9*, 739−746.
(51) Gladys, M. J.; El Zein, A. A.; Mikkelsen, A.; Andersen, J. N.; Held, G. *Surf. Sci.* **2008**, *602*, 3540−3549.
(52) Hodgson, A.; Haq, S. *Surf. Sci. Rep.* **2009**, *64*, 381−451.
(53) Meng, S.; Wang, E. G.; Gao, S. *Phys. Rev. B* **2004**, *69*, 195404.
(54) Doering, D. L.; Poppa, H.; Dickinson, J. T. *J. Catal.* **1982**, *73*, 104−119.
(55) Stara, I.; Matolin, V. *Surf. Sci.* **1994**, *313*, 99−106.
(56) Rainer, D. R.; Wu, M.-C.; Mahon, D. I.; Goodman, D. W. *J. Vac. Sci. Technol., A* **1996**, *14*, 1184−1188.
(57) Matolin, V.; Gillet, E. *Surf. Sci.* **1990**, *238*, 75−82.
(58) Wilde, M.; Fukutani, K.; Ludwig, W.; Brandt, B.; Fischer, J.-H.; Schauermann, S.; Freund, H.-J. *Angew. Chem., Int. Ed.* **2008**, *47*, 9289−9293.
(59) Neyman, K. M.; Schauermann, S. *Angew. Chem., Int. Ed.* **2010**, *49*, 4743−4746.
(60) Gracia, L.; Calatayud, M.; Andrés, J.; Minot, C.; Salmeron, M. *Phys. Rev. B* **2005**, *71*, 033407.
(61) Yudanov, I. V.; Neyman, K. M.; Rösch, N. *Phys. Chem. Chem. Phys.* **2004**, *6*, 116−123.
(62) Behm, R. J.; Christmann, K.; Ertl, G.; Van Hove, M. A. *J. Chem. Phys.* **1980**, *73*, 2984−2995.
(63) Jeon, T.-Y.; Yoo, S. J.; Park, H.-Y.; Kim, S.-K.; Lim, S.; Peck, D.; Jung, D.-H.; Sung, Y.-E. *Langmuir* **2012**, *28*, 3664−3670.
(64) Barth, C.; Claeys, C.; Henry, C. R. *Rev. Sci. Instrum.* **2005**, *76*, 083907.
(65) Barth, C.; Henry, C. R. *Nanotechnology* **2006**, *17*, S155−S161.
(66) *Gwyddion*, 2014 (http://gwyddion.net/).
(67) Ooi, N.; Rairkar, A.; Adams, J. B. *Carbon* **2006**, *44*, 231−242.
(68) Michaelson, H. B. *J. Appl. Phys.* **1977**, *48*, 4729−4733.
(69) Schäfer, A.; Shumay, I. L.; Wiets, M.; Weinelt, M.; Fauster, Th.; Chulkov, E. V.; Silkin, V. M.; Echenique, P. M. *Phys. Rev. B* **2000**, *61*, 13159−13163.
(70) Fischer, R.; Schuppler, S.; Fischer, N.; Fauster, Th.; Steinmann, W. *Phys. Rev. Lett.* **1993**, *70*, 654−657.
(71) Kubiak, G. D. *J. Vac. Sci. Technol., A* **1987**, *5*, 731−734.
(72) Methfessel, M.; Hennig, D.; Scheffler, M. *Phys. Rev. B* **1992**, *46*, 4816−4829.
(73) Pallassana, V.; Neurock, M.; Hansen, L. B.; Hammer, B.; Nørskov, J. K. *Phys. Rev. B* **1999**, *60*, 6146−6154.